J Mater Sci: Mater Electron (2017) 28:17551–17556
DOI 10.1007/s10854-017-7691-y

Simple 3,6-bis(diphenylaminyl)carbazole molecular glasses as hole transporting materials for hybrid perovskite solar cells

Thanh-Tuân Bui[1] · Fabrice Goubard[1] · Joel Troughton[2] · Trystan Watson[2]

Received: 1 July 2017 / Accepted: 10 August 2017 / Published online: 22 August 2017

Abstract 3,6-bis(diphenylaminyl)carbazole molecular glasses were initially designed as solid hole conductor for solid-state dye-sensitized solar cells. Herein we employed these simple and easy-to-synthesize carbazole derivatives in $CH_3NH_3PbI_3$ regular perovskite solar cells. Devices using these hole transporting materials (HTM) gave comparable efficiency to the conventional Spiro-OMeTAD based control device made under the same conditions, thus demonstrating the huge potential of carbazole-based molecular glasses as an emerging class of lower cost organic hole conductors with easier synthetic pathways for solid state hybrid solar cells.

1 Introduction

In the last 10 years, the rise of perovskite solar cells (PSC) has been one of the most impressive evolutions in the history of photovoltaic technology. Their power conversion efficiency (PCE) rose from 3.8% in 2009 to higher than 22% in mid 2016 for single cells [1]. Importantly, these solar cells are prepared by soft techniques using solution processing. Therefore, the cost-effective large-scale production of PSC seems to be realizable. For instance, Di Giacomo et al. [2] successfully demonstrated flexible perovskite photovoltaic modules using low-temperature processes including UV-irradiation of the mesoporous TiO_2 and atomic layer deposition of the compact TiO_2 giving solar cells with 8.4% efficiency, good flexibility, and improved stability with respect to scaffoldless equivalents. Screen-printable scaffolds and masking/laser patterning procedures enables fabrication of 3.1%-efficient mesostructured perovskite modules on plastic substrates.

In PSC, the hybrid perovskite light harvesting layer as well as materials for selective contacts serving electron and hole extraction are the most important components. The use of HTMs to extract holes from perovskite and to transport them to the electrode, is indispensable in almost all the architectures utilized for PSCs [3]. Spiro-OMeTAD (Fig. 1) has been the most commonly used HTM for PSCs. Originally used in solid-state dye sensitized solar cells (DSSC) research [4, 5], it has been successfully adapted for PSC and has shown PCE over 22%. However, the onerous synthetic pathway and costs of Spiro-OMeTAD is an obstacle for large-scale production [6]. For this reason, alternative cost-effective HTMs for highly efficient PSCs are highly researched. In search of alternatives to Spiro-OMeTAD, a huge number of molecular HTMs have been employed in PSC [7–9]. A dozen of them have been found to give devices with performance comparable, or even superior, to that of Spiro-OMeTAD (PCE ~20%.) [10–15]. Among them, carbazole derivatives are attractive classes of HTMs [16–20]. This is due to their interesting properties, including suitable electrochemical oxidation potentials, good charge transport, and good thermal and morphological stability. Recently, we have developed a series of carbazole based hole conductors, which are easily prepared in a short synthetic pathway, for solid state DSSC [17]. Herein we show that these materials are also suitable for elaboration of efficient $CH_3NH_3PbI_3$ PSCs, leading to efficient devices with

✉ Thanh-Tuân Bui
tbui@u-cergy.fr

Trystan Watson
t.m.watson@swansea.ac.uk

[1] Laboratoire de Physicochimie des Polymères et des Interfaces (LPPI), Université de Cergy-Pontoise, 5 mail Gay Lussac, 95000 Neuville-sur-Oise, France

[2] SPECIFIC, Swansea University Bay Campus, Fabian Way, Swansea SA1 8EN, UK

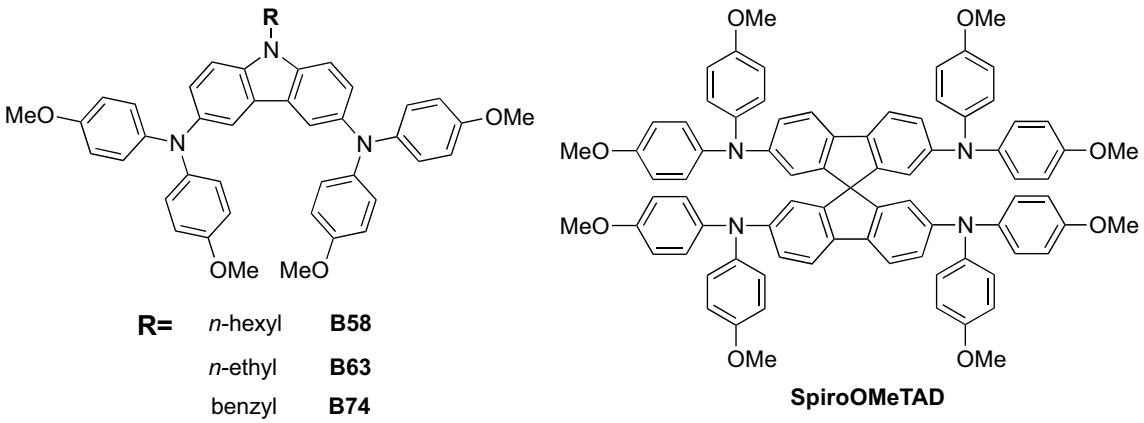

Fig. 1 Molecular structures of studied hole transporters

comparable performance to Spiro-OMeTAD under standard conditions.

2 Results and discussion

2.1 Materials synthesis

The structure of the studied hole transporters are given in Fig. 1. Structurally, *N*-alkylated carbazoles are end-capped by di(4-methoxyphenyl)amino function in 3,6 positions. These electron rich groups will modulate optoelectrochemical properties of targeted compounds. Methoxy groups render molecules more soluble in organic solvents. Additionally, the presence of methoxy groups in para positions of phenyl rings of the diphenylamino moiety favour charge transport properties [21, 22]. It is reported that the alkyl chain at *N*-position of carbazole favours the infiltration into mesoporous networks [23].

The materials can be easily synthesized in short synthetic sequence from readily available commercial products (Fig. 2). Briefly, 3,6-dibromocarbazoles react with alkyl halide in basic medium leading to *N*-alkyl-3,6-dibromocarbazoles. The latter is the subjected to a twofold Pd-catalyzed amination with 4,4′-dimethoxydiphenylamine, leading to the final products in good yields [17].

These carbazole derivatives have good solubility in organic solvents (such as toluene, chlorobenzene, etc.), rendering them suitable for PSC elaboration by wet-process.

2.2 Thermal and optoelectrochemical properties

The thermal and optoelectrochemical properties of these compounds have been previously reported [17]. All compounds showed significant thermal stability ($T_d > 300$ °C), suitable for the applications in optoelectronic devices and the glass transition temperature (T_g) range from 55 to 80 °C, depending on the length of alkyl chain at the *N*-position: shorter chain leads to higher molecular rigidity, and as consequence higher T_g. The presence of the amorphous phase is highly desirable for producing a homogeneous, compact film with good HTM/perovskite interfacial contact, which is vital

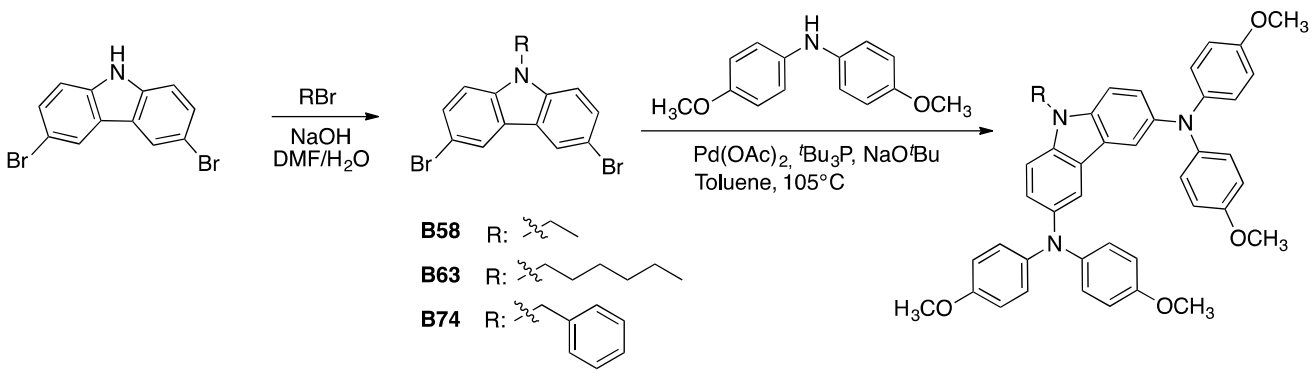

Fig. 2 Synthesis of carbazole HTMs

for efficient charge transfer, thus leading to high efficiency. Analysis by cyclic voltammetry suggests that these molecules are electrochemically stable. The ionization potentials (IPs) were estimated from the onset of the first oxidation. The electron affinity (EAs) was estimated by subtracting the optical bandgap from the IPs. These data are summarised in Table 1, together with that of Spiro-OMeTAD obtained under identical conditions. Carbazole compounds have IPs and EAs close to that of Spiro-OMeTAD measured under the same conditions. Their HOMO level is located above the ground-state level of the $CH_3NH_3PbI_3$ absorber (5.4 eV), thus ensuring efficient charge extraction and transferability. Additionally, the hydrophobicity of *N*-alkyl substituted carbazole hole conductors has been proved to improve moisture resistance in hybrid perovskite based devices [24]. All these characteristics suggest that these materials will be suitable for use as HTM in PSC.

2.3 Photovoltaic performance

Carbazole compounds were then incorporated as HTM in regular $CH_3NH_3PbI_3$ PSC devices. A typical PSC device is demonstrated in Fig. 3, illustrating an optimized device composed of a compact TiO_2 (50 nm), mesoporous TiO_2 (250 nm) filled with $CH_3NH_3PbI_3$ perovskite (50 nm of capping layer), HTM (100 nm) and a 100 nm thermally evaporated Au layer as cathode.

Molecular glasses have been known for having low charge mobility in pristine state. The intrinsic charge transport properties of B58, B63 and B74 were investigated in field effect transistors using these molecules as active layers together with Spiro-OMeTAD as reference [17]. B58 has slightly higher mobility ($2.87.10^{-7}$ cm^2/Vs at 1 V) than that of B63 ($1.77.10^{-7}$ cm^2/Vs at 1 V), probably due to better molecular packing in the film. B74 have the lowest mobility ($1.18.10^{-7}$ cm^2/Vs at 1 V) due to the worst molecular packing in solid state. These are in line with our observation in the absorption spectra of the films where B74 showed the weakest intensity at the transition correlating to π–π stacking. However, Spiro-OMeTAD showed about one order of magnitude higher mobility (2.10^{-6} cm^2/Vs at 1 V) than those of these carbazoles.

We thus incorporated 4-*tert*-butylpyridine (*t*BP) and bis(trifluoromethane)sulfonamide lithium salt (LiTFSI) in the HTM solution for making photovoltaic devices. *t*BP increases the polarity of HTM and enhances the interfacial contact between perovskite/HTM, leading to a high V_{oc} and PCE [25]. *t*BP acts also as a charge recombination inhibitor

Table 1 Thermal, optoelectrochemical and photovoltaic properties of studied materials

Compound	T_g/T_d (°C)	IP (eV)	EA (eV)	μ_h (cm^2 V^{-1} s^{-1})	Scan direction	J_{sc} (mA cm^{-2})	V_{oc} (V)	FF (%)	PCE (%)
B63	80/375	4.70	1.93	1.77×10^{-7}	$V_{oc}\rightarrow J_{sc}$	18.6	0.878	59.2	10.8
					$J_{sc}\rightarrow V_{oc}$	16.7	0.845	41.1	6.4
B58	55/398	4.65	1.85	2.87×10^{-7}	$V_{oc}\rightarrow J_{sc}$	13.7	0.836	59.3	7.5
					$J_{sc}\rightarrow V_{oc}$	12.9	0.751	51.8	5.6
B74	66/336	4.68	1.91	1.18×10^{-7}	$V_{oc}\rightarrow J_{sc}$	17.5	0.931	54.7	9.9
					$J_{sc}\rightarrow V_{oc}$	16.9	0.911	48.3	8.3
Spiro-OMeTAD		4.70	1.70	2×10^{-6}	$V_{oc}\rightarrow J_{sc}$	15.8	0.921	69.2	11.2
					$J_{sc}\rightarrow V_{oc}$	15.5	0.912	65.0	10.2

The T_d, T_g, IP, EA, μ_h are from our previous work [17]

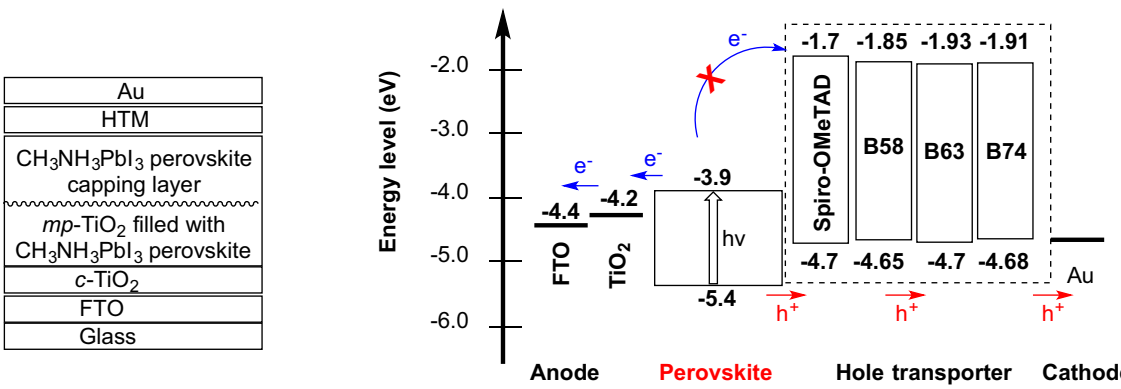

Fig. 3 General PSC device structure (*left*) and energy levels of the device components (*right*)

and prevents phase segregation of LiTFSI and HTM, resulting in a homogeneous hole transport layer. These properties are critical for charge transport in the HTL bulk film as well as at the perovskite/HTM and HTM/electrode interfaces for efficient PSC [26, 27]. LiTFSI is known to act as an oxidative agent in the presence of oxygen and moisture, and increase the hole mobility of molecular HTM [28, 29].

The current-density–voltage (J–V) characteristics of the perovskite solar cells and the J–V curve statistics for devices employing different carbazole hole transport materials are shown in Figs. 4 and 5, respectively. For comparison, the control devices with Spiro-OMeTAD were also fabricated, and the measured data are summarized in Table 1.

The device incorporating B58 achieves a short-circuit current (J_{sc}) of 13.7 mA cm^{-2}, an open-circuit voltage (V_{oc}) of 0.836 V, a fill factor (FF) of 59%, giving an overall conversion efficiency of 7.5% (Figs. 4 and 5). The B63 based cells shown 10.8% efficiency due to higher J_{sc} (18.6 mA cm^{-2}) and V_{oc} (0.878 V). The benzyl substituted B74 gave highest Voc (0.931 V). However, due to the drop of FF, the PCE decreases to 9.9%. These PCE are slightly lower to that of Spiro-OMeTAD control devices (11.2%). However, the hysteresis effect of carbazole based HTMs are more prominent in comparison to Spiro-OMeTAD. That may be attributed to the lower mobility of these materials (Table 1).

The IPCE spectra of PSC are presented in Fig. 6 and the values of integrated J_{sc} are given in the inset of this figure. The values are in perfect accordant with measured J_{sc} from I–V curves: 14.69; 16.67; 16.07 and 17.03 mA cm^{-2} for B58, B63, B74 and Spiro-OMeTAD based PSC respectively.

3 Conclusions

In summary, we have successfully applied three *N*-alkyl substituted bis(diphenylaminyl)carbazoles as HTM in $CH_3NH_3PbI_3$ PSC. These materials gave PSC with performance comparable to that of the reference materials (Spiro-OMeTAD) prepared under the same conditions. The higher hysteresis effect of these materials could be attributed to their lower charge mobility in comparison to Spiro-OMeTAD. Our results thus affirm the successful application of simple molecular HTM materials designed for solid-state DSSCs in hybrid perovskite photovoltaics.

3.1 Experimental

Etched FTO glass substrates (NSG Pilkington, TEC7) were cleaned sequentially in detergent, deionised water, acetone and ethanol before undergoing 10 min of O_2 plasma treatment. A compact TiO_2 layer was deposited on the glass substrates through spray pyrolysis of a 0.2 M solution of titanium diisopropoxide bis(acetylacetonate) in isopropanol at 450 °C. Upon cooling, a mesoporous layer of TiO_2 nanoparticles was spin-coated from a 2:7 wt suspension of Dyesol

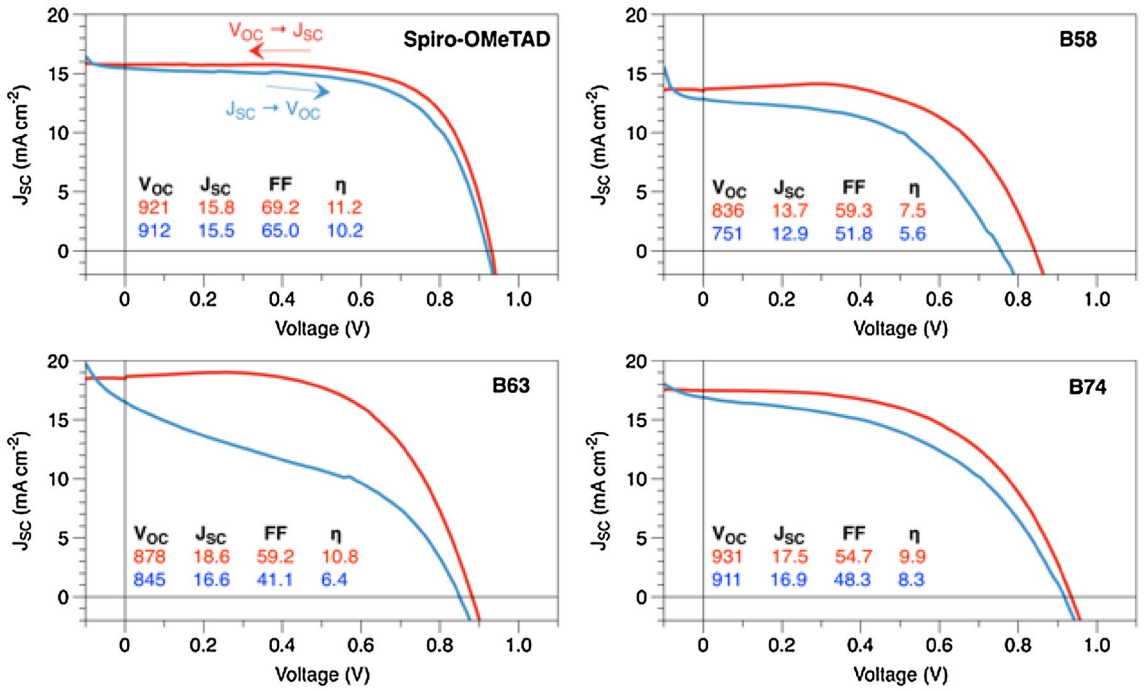

Fig. 4 Current density–voltage (J–V) curves of best PSC devices

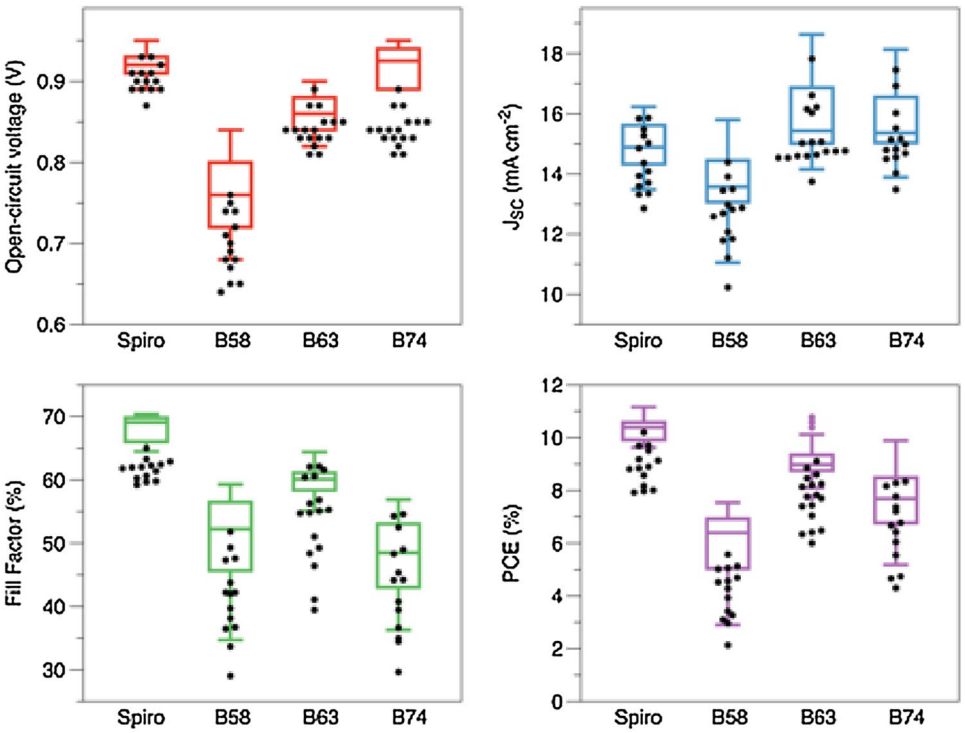

Fig. 5 Current–voltage curve statistics for devices employing different hole transport materials. *Solid boxes* represent data gathered during a V_{OC} to J_{SC} sweep, whereas *black points* represent data from the J_{SC} to V_{OC} sweep. The difference between the two data sets indicates the degree of J–V hysteresis within devices

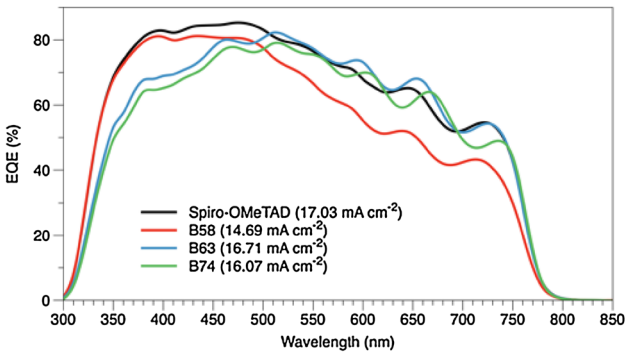

Fig. 6 IPCE spectra of the best PSC devices

30NR-D paste in ethanol (4500 rpm for 30 s), followed by sintering at 550 °C for 30 min.

A $CH_3NH_3PbI_3$ perovskite precursor solution was prepared by dissolving 576 mg PbI_2, and 199 mg CH_3NH_3I in a 4:1 vol solution of DMF:DMSO. 100 µl of the perovskite precursor solution was deposited onto the TiO_2 films and spin-coated at 4000 rpm for 30 s, with 200 µl of ethyl acetate dripped onto the spinning substrate 10 s prior to the end of the spin-coating process. Perovskite films were annealed at 100 °C for 10 min.

Hole transport materials were dissolved in chlorobenzene (75 mg/ml) and doped with additives including bis(trifluoromethylsulfonyl)imide lithium salt (Li-TFSI, 20 µl/ml from a 1.8 M solution in acetonitrile) and 4-tert-butylpyridine (tBP, 30 µl/ml). The HTM solution was spin-coated onto perovskite films at 4500 rpm for 30 s before 100 nm thick Au contacts were thermally evaporated onto devices.

Current–voltage measurements were performed using a AAA-rated solar simulator (Oriel Sol3A) calibrated against a KG5-filtered reference diode (Oriel 91,150-KG5). Solar cells were masked to 0.1 cm^2 and scanned both from forward to reverse bias and vice versa at 100 mV/s.

Acknowledgements The authors would like to acknowledge support from the Engineering and Physical Sciences Research Council SPACE-Modules project (EP/M015254/1).

References

1. A. Kojima, K. Teshima, Y. Shirai, T. Miyasaka, J. Am. Chem. Soc. **131**, 6050–6051 (2009)
2. F. Di Giacomo, V. Zardetto, A. D'Epifanio, S. Pescetelli, F. Matteocci, S. Razza, A. Di Carlo, S. Licoccia, W.M.M. Kessels, M. Creatore, T.M. Brown, Adv. Energy Mater. **5**(8), 1401808 (2015)
3. H.S. Kim, I.H. Jang, N. Ahn, M. Choi, A. Guerrero, J. Bisquert, N.G. Park, J. Phys. Chem. Lett. **6**(22), 4633–4639 (2015)
4. U. Bach, D. Lupo, P. Comte, J.E. Moser, F. Weissörtel, J. Salbeck, H. Spreitzer, M. Grätzel, Nature **395**(6702), 583–585 (1998)
5. J. Burschka, A. Dualeh, F. Kessler, E. Baranoff, N.-L. Cevey-Ha, C. Yi, M.K. Nazeeruddin, M. Grätzel, J. Am. Chem. Soc. **133**(45), 18042–18045 (2011)
6. M.L. Petrus, T. Bein, T.J. Dingemans, P. Docampo, J. Mater. Chem. A **3**(23), 12159–12162 (2015)
7. Z. Yu, L. Sun, Adv. Energy Mater. **5**(12), 1500213 (2015)

8. S. Ameen, M.A. Rub, S.A. Kosa, K.A. Alamry, M.S. Akhtar, H.-S. Shin, H.-K. Seo, A.M. Asiri, M.K. Nazeeruddin, ChemSusChem **9**(1), 10–27 (2016)
9. L. Calió, S. Kazim, M. Grätzel, S. Ahmad, Angew. Chem. Int. Ed. **55**(47), 14522–14545 (2016)
10. D. Bi, B. Xu, P. Gao, L. Sun, M. Grätzel, A. Hagfeldt, Nano Energy **23**, 138–144 (2016)
11. Y. Hua, J. Zhang, B. Xu, P. Liu, M. Cheng, L. Kloo, E.M.J. Johansson, K. Sveinbjörnsson, K. Aitola, G. Boschloo, L. Sun, Nano Energy **26**, 108–113 (2016)
12. M. Daskeviciene, S. Paek, Z. Wang, T. Malinauskas, G. Jokubauskaite, K. Rakstys, K.T. Cho, A. Magomedov, V. Jankauskas, S. Ahmad, H.J. Snaith, V. Getautis, M.K. Nazeeruddin, Nano Energy **32**, 551–557 (2017)
13. I. Zimmermann, J. Urieta-Mora, P. Gratia, J. Aragó, G. Grancini, A. Molina-Ontoria, E. Ortí, N. Martín, M.K. Nazeeruddin, Adv. Energy Mater. **7**(6), 1601674 (2017)
14. T. Malinauskas, M. Saliba, T. Matsui, M. Daskeviciene, S. Urnikaite, P. Gratia, R. Send, H. Wonneberger, I. Bruder, M. Graetzel, V. Getautis, M.K. Nazeeruddin, A. Hagfeldt, G. Pozzi, M. Graetzel, M.K. Nazeeruddin, Energy Environ. Sci. **9**(5), 1681–1686 (2016)
15. B. Xu, D. Bi, Y. Hua, P. Liu, M. Cheng, M. Grätzel, L. Kloo, A. Hagfeldt, L. Sun, W. Zhang, A. Hagfeldt, L. Sun, M.K. Nazeeruddin, M. Grätzel, A. Hagfeldt, Energy Environ. Sci. **9**(3), 873–877 (2016)
16. L. Calió, C. Momblona, L. Gil-Escrig, S. Kazim, M. Sessolo, Á. Sastre-Santos, H.J. Bolink, S. Ahmad, Sol. Energy Mater. Sol. Cells **163**, 237–241 (2017)
17. T.-T. Bui, S.K. Shah, M. Abbas, X. Sallenave, G. Sini, L. Hirsch, F. Goubard, ChemNanoMat 1(3), 203–210 (2015)
18. T.-T. Bui, F. Goubard, EPJ Photovoltaics **4**, 40402 (2013)
19. T.T. Bui, L. Beouch, X. Sallenave, F. Goubard, Tetrahedron Lett. **54**(32), 4277–4280 (2013)
20. Y. Xue, Y. Wu, Y. Li, J. Power Sources **344**, 160–169 (2017)
21. V. Mimaite, J. Ostrauskaite, D. Gudeika, J.V. Grazulevicius, V. Jankauskas, Synth. Met. **161**(15), 1575–1581 (2011)
22. A. Sakalyte, J. Simokaitiene, A. Tomkeviciene, J. Keruckas, G. Buika, J.V. Grazulevicius, V. Jankauskas, C.-P. Hsu, C.-H. Yang, J. Phys. Chem. C **115**(11), 4856–4862 (2011)
23. M. Manaa, S. Ben; Benhattab, B. Schmaltz, N. Berton, J. Bouclé, A. Lamine, F.T. Ben; Van, Mediterr. J. Chem. **5**(6), 599–604 (2016)
24. T. Leijtens, T. Giovenzana, S.N. Habisreutinger, J.S. Tinkham, N.K. Noel, B.A. Kamino, G. Sadoughi, A. Sellinger, H.J. Snaith, ACS Appl. Mater. Interfaces **8**(9), 5981–5989 (2016)
25. W. Li, H. Dong, L. Wang, N. Li, X. Guo, J. Li, Y. Qiu, J. Mater. Chem. A **2**(33), 13587 (2014)
26. S. Wang, M. Sina, P. Parikh, T. Uekert, B. Shahbazian, A. Devaraj, Y.S. Meng, Nano Lett. **16**(9), 5594–5600 (2016)
27. E.J. Juarez-Perez, M.R. Leyden, S. Wang, L.K. Ono, Z. Hawash, Y. Qi, Chem. Mater. **28**(16), 5702–5709 (2016)
28. A.-N. Cho, H.-S. Kim, T.-T. Bui, X. Sallenave, F. Goubard, N.-G. Park, RSC Adv. **6**(72), 68553–68559 (2016)
29. Z. Hawash, L.K. Ono, Y. Qi, Adv. Mater. Interfaces **3**(13), 1600117 (2016)